

H. Narayanan · E. Arruda · K. Grosh · K. Garikipati

Biological growth: Reaction, transport and mechanics

Theory and Numerical Models

“Tact is the knack of making a point without making an enemy” (v0.7)

Received: date / Accepted: date

Abstract In this paper, we address some modelling issues related to biological growth. Our treatment is based on a recently-proposed general formulation for growth (Journal of the Mechanics and Physics of Solids, **52**, 2004, 1595–1625) within the context of open system continuum thermodynamics. We aim to enhance this treatment by making it more appropriate for the biophysics of growth in soft tissue, specifically tendon. This involves several modifications to the mathematical formulation to represent the reactions, transport and mechanics, and their interactions. We also reformulate the governing differential equations for reaction-transport to represent the incompressibility constraint on the fluid phase of the tissue. This revision enables a straightforward implementation of numerical stabilisation for the hyperbolic, or advection-dominated, limit. A finite element implementation employing a staggered scheme is utilised to solve the coupled nonlinear partial differential equations that arise from the theory. Motivated by our experimental model, an *in vitro* scaffold-free engineered tendon formed by self-assembly of tendon fibroblasts (Calve et al, 2004), several numerical examples are solved in this context demonstrating biophysical aspects of growth, and the improved numerical performance of the models.

Keywords Soft Tissue · Porous Media · Enzyme Kinetics · Advection-Diffusion · Incompressibility · Stabilisation

1 Introduction

Growth involves the addition or depletion of mass in biological tissue. In biological systems, growth occurs in combination with *remodelling*, which is a change in microstructure, and possibly with *morphogenesis*, which is a change in form in the embryonic state. The physics of these processes are quite distinct, and for modelling purposes can,

and must, be separated. Our previous work (Garikipati et al, 2004), upon which we now seek to build, drew in some measure from Cowin and Hegedus (1976); Epstein and Maugin (2000); Taber and Humphrey (2001) and Kuhl and Steinmann (2003), and was focused upon a comprehensive account of the coupling between transport and mechanics. The origins of this coupling were traced to the balance equations, kinematics and constitutive relations. A major contribution of that work was the identification and discussion of several driving forces for transport that are thermodynamically-consistent, in the sense that specification of these relations does not violate the Clausius-Duhem dissipation inequality. Now, we seek to restrict the range of physically-admissible possibilities in order to gain greater physiological relevance for modelling growth in soft biological tissue. In addition, these refinements result in advection-diffusion equations for mass transport, which require numerical stabilisation in the advection-dominated regime (the hyperbolic limit). We draw upon the enforcement of the incompressibility limit for the fluid phase to facilitate this process. Below, we briefly introduce each aspect that we have considered, but postpone details until relevant sections in the paper.

- For a tissue undergoing finite strains, the transport equations can be formulated, mathematically, in terms of concentrations with respect to either the reference or current (deformed) configurations. However, the physics of fluid-tissue interactions and the imposition of relevant boundary conditions is best understood and represented in the current configuration.
- The state of saturation is crucial in determining whether the tissue swells and shrinks with infusion/expulsion of fluid.
- The fluid phase, whether slightly compressible or incompressible, can develop compressive stress without bound. However, it can develop at most a small tensile stress, having implications for the tissue’s stiffness and strength in tension as against compression. It also has implications for void formation through cavitation.
- When modelling transport, it is common to assume Fickian diffusion (Kuhl and Steinmann, 2003). This requires

that a mixing entropy be defined via the configurations available to molecules of the diffusing species at fixed values of a macroscopic variable, such as concentration. With regard to the extra-cellular fluid (ECF) or the chemical solutes dissolved in it, the state of saturation directly influences this mixing entropy.

- If fluid saturation is maintained, void formation in the pores is disallowed under an increase in the pores' volume. This has implications for the fluid exchanges between a deforming tissue and a fluid bath with which it is in contact.
- Recognising the incompressibility of the fluid phase, it is common to treat soft biological tissue as either incompressible or nearly-incompressible (Fung, 1993). At the scale of the pores (the microscopic scale in this case), however, a distinction exists in that the fluid is exactly (or nearly) incompressible, while the solid forming the porous network is not.
- In Garikipati et al (2004), the acceleration of the solid phase was included as a driving force in the constitutive relation for the flux of other phases. However, acceleration is non-objective and its use in constitutive relations is inappropriate.
- Chemical solutes in the ECF are advected by the fluid velocity and additionally undergo transport under a chemical potential gradient relative to the fluid. In the hyperbolic limit, where advection dominates, spatial instabilities are obtained in numerical solutions of the transport equation (Brooks and Hughes, 1982; Hughes et al, 1987). Numerical stabilisation of the equations is intimately tied to the mathematical representation of fluid incompressibility.

These issues are treated in detail in relevant sections of the paper, which is laid out as follows: Balance equations and kinematics are discussed in Section 2, constitutive relations for reactions, transport and mechanics in Section 3, and numerical examples are presented in Section 4. Conclusions are drawn in Section 5.

2 Balance equations and kinematics of growth

In this section, the coupled, continuum balance equations developed from physical principles governing the behaviour of growing tissue are summarised and specialised as outlined in Section 1. For detailed continuum mechanical arguments underlying the equations, the interested reader is directed to Garikipati et al (2004).

The tissue of interest is an open subset of \mathbb{R}^3 with a piecewise smooth boundary. At a reference placement of the tissue, Ω_0 , points in the tissue are identified by their reference positions, $X \in \Omega_0$. The motion of the tissue is a sufficiently smooth bijective map $\varphi : \overline{\Omega}_0 \times [0, T] \rightarrow \mathbb{R}^3$, where $\overline{\Omega}_0 := \Omega_0 \cup \partial\Omega_0$. At a typical time $t \in [0, T]$, $\varphi(X, t)$ maps a point X to its current position, x . In its current configuration, the tissue occupies a region $\Omega_t = \varphi_t(\Omega_0)$. These details are

depicted in Figure 1. The deformation gradient $F := \partial\varphi/\partial X$ is the tangent map of φ .

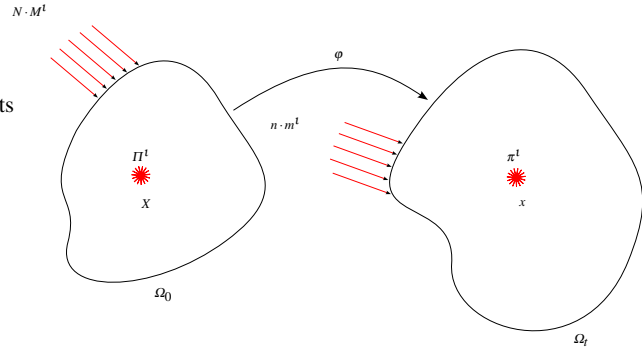


Fig. 1 The continuum tissue with growing and diffusing species.

The tissue consists of numerous species, of which the following groupings are of importance for the models: A *solid* species, consisting of solid collagen fibrils and cells,¹ denoted by c , an extra-cellular *fluid* species denoted by f and consisting of water bound to proteoglycans, and *solute* species, consisting of precursors to reactions, byproducts, nutrients, and other regulatory chemicals. A generic solute will be denoted by s . In what follows, an arbitrary species will be denoted by ι , where $\iota = c, f, s$.

The fundamental quantities of interest are mass concentrations, $\rho_0^{\iota}(X, t)$. These are the mass of each species per unit system volume in Ω_0 . Formally, these quantities can also be thought of in terms of the maps $\rho_0^{\iota} : \Omega_0 \times [0, T] \rightarrow \mathbb{R}$, upon which the formulation imposes some smoothness requirements. By definition, the total material density of the tissue at a point is a sum of these concentrations over all species $\sum_{\iota} \rho_0^{\iota} = \rho_0$. Other than the solid species, c , all phases have mass fluxes, M^{ι} . These are mass flow rates per unit cross-sectional area in the reference configuration *defined relative to the solid phase*. Except for the fluid, f , all species have mass sources/sinks, Π^{ι} , encapsulating the complexity of the biochemistry.

2.1 Balance of mass for an open system

As a result of mass transport and inter-conversion of species introduced previously, the concentrations, ρ_0^{ι} , change with time. In local form, the balance of mass for an arbitrary species in the reference configuration is

$$\frac{\partial \rho_0^{\iota}}{\partial t} = \Pi^{\iota} - \text{DIV}[M^{\iota}], \forall \iota, \quad (1)$$

recalling that, in particular, $M^s = \mathbf{0}$ and $\Pi^f = 0$. Here, $\text{DIV}[\bullet]$ represents the divergence operator in the reference configuration.

¹ At this point, we do not distinguish the solid species further. This is a good approximation to the physiological setting for tendons, which are relatively acellular and whose dry mass consists of up to 70% collagen.

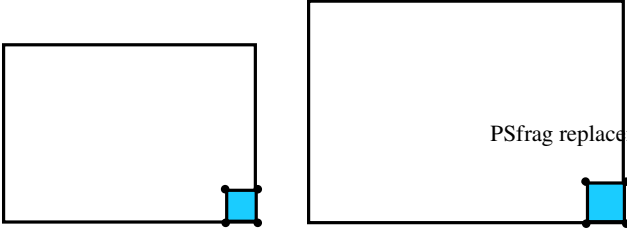


Fig. 2 If the pore structure at the boundary deforms with the tissue and this boundary is in contact with a fluid bath, the fluid concentration with respect to the current configuration, i.e., ρ^t , remains constant.

ration. The functional forms of Π^t are chosen to represent the underlying biochemistry (physiologically relevant examples of which are discussed in Section 3.4) and the fluxes, M^t , are determined from the thermodynamically motivated constitutive relations described in Section 3.3.

The behaviour of the entire system can be determined by summing Equation (1) over all species t . Additionally, sources and sinks satisfy the relation

$$\sum_t \Pi^t = 0, \quad (2)$$

which is consistent with the Law of Mass Action for reaction rates (Garikipati et al, 2004) and with mixture theory (Truesdell and Noll, 1965).

2.1.1 The role of mass balance in the current configuration

Though it is not mathematically incorrect to solve the initial-boundary-value problem in terms of Equation (1) written out for the various species, it is important to note that, as soft tissues deform, the current configuration, Ω_t , and its boundary, $\partial\Omega_t$, change in time. As the pore structure at the boundary deforms with the tissue, the fluid concentration with respect to Ω_t remains constant if the boundary is in contact with a fluid bath. Accordingly, this is the appropriate Dirichlet boundary condition to impose. This is shown in an idealised manner in Figure 2.

In order to apply boundary conditions (either specification of species flux or concentration) that are physical, it is straightforward to use the local form of the balance of mass in the current configuration,

$$\frac{d\rho^t}{dt} = \pi^t - \text{div}[m^t] - \rho^t \text{div}[v], \quad \forall t, \quad (3)$$

where $\rho^t(x, t)$, $\pi^t(x, t)$, and $m^t(x, t)$ are the current mass concentration, source and mass flux of species t respectively. $\text{div}[\bullet]$ is the spatial divergence operator, and the time derivative on the left hand-side in Equation (3) is the material time derivative, that may be written explicitly as $\frac{\partial}{\partial t}|_X$, implying that the reference position is held fixed.

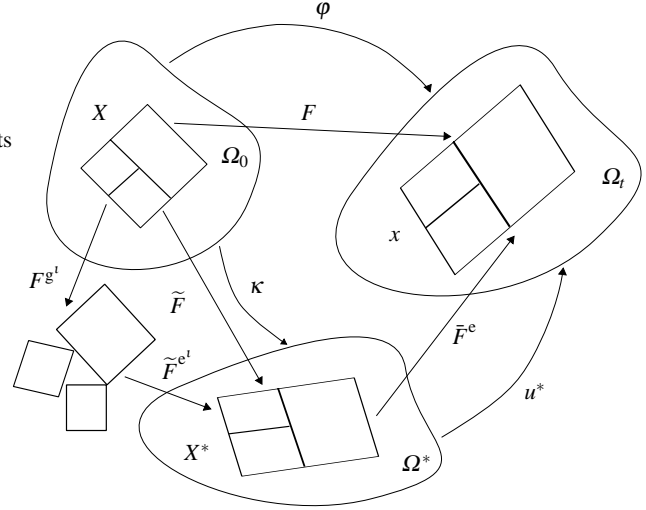


Fig. 3 The kinematics of growth.

2.2 The kinematics of growth

Local volumetric changes are associated with changes in the concentrations of species. The material of the species swells with an increase in concentration, and shrinks as its concentration decreases. This leads to the notion of a *growth deformation gradient*. One aspect of the coupling between mass transport and mechanics stems from this phenomenon. In the setting of finite strain kinematics, the total deformation gradient is decomposed into the growth deformation gradient, a *geometrically-necessitated elastic deformation* accompanying growth, and an *additional elastic deformation due to external stress*. This split is analogous to the classical decomposition of multiplicative plasticity (Lee, 1969) and is similar to the approach followed in existing literature on biological growth (see, for e.g., Taber and Humphrey (2001); Ambrosi and Mollica (2002)).

The split itself is visualised in Figure 3. Assuming that the volume changes associated with growth described above are isotropic, a simple form for the growth deformation gradient tensor is

$$F^{g^t} = \frac{\rho_0^t}{\rho_{0_{\text{ini}}}^t} \mathbf{1}, \quad (4)$$

where $\rho_{0_{\text{ini}}}^t(X)$ can be interpreted as an original reference state where the species would be stress free in the absence of a deformation, and $\mathbf{1}$ is the second-order isotropic tensor. Additionally, this being a local definition, the action of F^{g^t} alone can result in incompatibility. In order to ensure compatibility, there is a further geometrically-necessary elastic deformation \tilde{F}^{e^t} . Thus, the total deformation gradient $F = \tilde{F}^e \tilde{F}^{e^t} F^{g^t}$, (where \tilde{F}^e arises from the external stress) and internal stresses in the tissue arise due to the compatibility restoring tensor \tilde{F}^{e^t} .

2.2.1 Saturation and tissue swelling

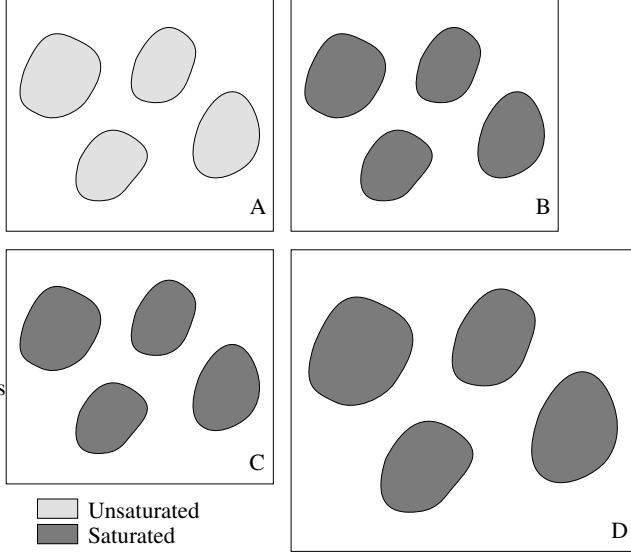


Fig. 4 Only under conditions of fluid saturation does an increase in fluid concentration cause tissue swelling.

Upon closer examination of the solid phase of the tissue as a porous medium, it is observed that its degree of saturation plays a fundamental role in determining whether the tissue responds by swelling or shrinking to an infusion or expulsion of fluid. In particular, the isotropic swelling law defined by Equation (4) has to be generalised to handle the case in which the solid phase is not saturated by fluid.

Figure 4 schematically depicts two potential scenarios. If the tissue is initially unsaturated (as in A), this corresponds to the fact that, on a microscopic scale, it still contains unfilled voids. It is thus capable of allowing an influx of fluid, which tends to increase its degree of saturation (to reach B), but does not cause the tissue to swell, as the incoming fluid particles occupy the available spaces. However, if we were to start observing the tissue at a point where it was initially saturated (as in C), an increase in the amount of fluid will result in swelling (as depicted in D), as there are no vacant locations for the entering fluid particles to occupy. It is this second case that is modelled by (4).

The measure of saturation we require to augment the isotropic swelling law to handle the unsaturated case arises naturally from our primary variables, the concentrations of the various species, ρ_0^t . These quantities can also be thought of as the product of the intrinsic density of the species, $\bar{\rho}_0^t$, and the corresponding volume fraction, \tilde{v}^t . Upon solution of the mass balance equation (1) for ρ_0^t , the species volume fractions, \tilde{v}^t , can be computed since the intrinsic densities are known material properties. The sum of these volume fractions is our required measure of saturation, and clearly cannot exceed unity. We thus proceed to redefine the growth deformation gradient tensor as follows:

$$F^{g^t} = \begin{cases} \mathbf{1}, & \sum_t \tilde{v}^t < 1 \\ \frac{\rho_0^t}{\rho_{0_{ini}^t}} \mathbf{1}, & \text{otherwise.} \end{cases} \quad (5)$$

However, it is important to note that under most physiological conditions, soft tissues are fully saturated by the fluid and can be modelled appropriately by Equation (4).

2.3 Balance of momenta

In soft tissues, the terms that appear on the right hand-side in Equation (1), the species production rate and flux, are strongly dependent on the local state of stress. To correctly model this coupling, the balance of linear momentum should be solved to determine the local state of strain and stress.

The deformation of the tissue is characterised by the map $\varphi(X, t)$. Recognising that, in tendons, the solid collagen fibrils and fibroblasts do not undergo mass transport, the material velocity of this species, $V = \partial\varphi/\partial t$, is used as the primitive variable for mechanics. The motion of the remaining species are split into a deformation along with the solid species, and mass transport relative to it. To this end, it is useful to define the material velocity of a species t relative to the solid skeleton as: $V^t = (1/\rho_0^t)FM^t$. Thus, the total material velocity of a species t is $V + V^t$. The total first Piola-Kirchhoff stress tensor, P , is the sum of the partial stresses P^t (borne by a species t) over all the species present.² With the introduction of these quantities, the balance of linear momentum in local form for a species t in Ω_0 is

$$\rho_0^t \frac{\partial}{\partial t} (V + V^t) = \rho_0^t (g + q^t) + \text{DIV}[P^t] - (\text{GRAD}[V + V^t])M^t, \quad (6)$$

where g is the body force per unit mass, and q^t is an interaction term denoting the force per unit mass exerted upon t by all other species present. The final term with the (reference) gradient denotes the contribution of the flux to the balance of momentum. In practise, the relative magnitude of the fluid mobility (and hence flux) is small, so the final term on the right hand side of Equation (6) is negligible, resulting in a more classical form of the balance of momentum. Furthermore, the absence of significant acceleration of the tissue during growth implies that the left hand-side can also be neglected, reducing (6) to the quasi-static balance of linear momentum.

The balance of momentum of the entire tissue is obtained by summing Equation (6) over all t . Additionally, recognising that the rate of change of momentum of the entire tissue is affected only by external agents and is independent of internal interactions, the following relation arises.

$$\sum_t (\rho_0^t q^t + \Pi^t V^t) = 0. \quad (7)$$

² The amino acids, nutrients and regulators are in solution at low concentrations, and do not bear any appreciable stress.

This is also consistent with classical mixture theory (Truesdell and Noll, 1965). See Garikipati et al (2004) for further details on balance of linear momentum, and the formulation of balance of angular momentum. We only note here that the latter principle leads to a symmetric partial Cauchy stress, σ^t for each species in contrast with the unsymmetric Cauchy stress of Epstein and Maugin (2000).

3 Constitutive framework and modelling choices

As is customary in field theories of continuum physics, the Clausius-Duhem inequality is obtained by multiplying the entropy inequality (the second law of thermodynamics) by the temperature field, θ , and subtracting it from the balance of energy (the first law of thermodynamics). We assume the internal energy per unit reference volume of species t to be of a sufficiently general form: $e^t = \hat{e}^t(F^{e^t}, \eta_0^t, \rho_0^t)$, where η_0^t is the entropy per unit system volume. Substituting this in the Clausius-Duhem inequality and applying the chain rule results in a form of this inequality that the specified constitutive relations *must not* violate. Only the valid constitutive laws relevant to the examples that follow are listed here. For details, see Garikipati et al (2004).

3.1 An anisotropic network model based on entropic elasticity

Each constituent of the tissue has a mass-specific Helmholtz free energy density, ψ^t . Utilising the material response of a hyperelastic material, the partial first Piola-Kirchhoff stress of collagen is $P^c = \rho^c \partial \psi^c / \partial F^c$. Here, $F^c = FF^g^{-1}$ is the elastic deformation gradient, and F^g is the growth deformation gradient, of collagen. Along the lines of Equation (4), if we were considering unidirectional growth of collagen along a unit vector e , we have $F^g = \frac{\rho_0^c}{\rho_0^c} e \otimes e$, with ρ_0^c denoting the initial concentration of collagen at the point.

The mechanical response (function) of tendons in tension is determined by their most important structural component, highly oriented fibrils of collagen. In our preliminary formulation, the strain energy density for the collagen has been obtained from hierarchical multi-scale considerations based upon an entropic elasticity-based worm-like chain (WLC) model (Kratky and Porod, 1949). The WLC model has been widely used for long chain single molecules, most prominently for DNA (Marko and Siggia, 1995; Rief et al, 1997; Bustamante et al, 2003), and recently for the collagen monomer (Sun et al, 2002). The central parameters of this model are the chain's contour length, L , and persistence length, A . The latter is a measure of its stiffness and given by $A = \chi/k\theta$, where χ is the bending rigidity, k is Boltzmann's constant and θ is the temperature (Landau and Lifshitz, 1951). We have fitted the WLC response function derived by Marko and Siggia (1995) to the data of Graham et al (2004) with $A = 6$ nm and $L = 3480$ nm. This is to be

compared with $A = 14.5$ nm and $L = 309$ nm, reported by Sun et al (2002), for a *single* collagen molecule. Taken together, these results demonstrate that the WLC analysis correctly predicts a collagen fibril to be longer and slightly more compliant than its constituent molecule due to compliant intermolecular cross-links in a fibril. To model the possibility of a collagen network structure, the WLC model has been embedded as a single constituent chain of an eight-chain model (Arruda and Boyce, 1993), depicted in Figure 5. Homogenisation via averaging then leads to a continuum strain energy function, ψ_F^c (the strain energy is one of the additive contributions to the Helmholtz free energy, ψ^c):

$$\begin{aligned} \tilde{\rho}^c \psi_F^c(F^e) &= \frac{Nk\theta}{4A} \left(\frac{r^2}{2L} + \frac{L}{4(1-r/L)} - \frac{r}{4} \right) \\ &+ \frac{\gamma}{\beta} (J^{e-2\beta} - 1) + \gamma \mathbf{1} : (C^e - \mathbf{1}) \\ &- \frac{Nk\theta}{4\sqrt{2L/A}} \left(\sqrt{\frac{2A}{L}} + \frac{1}{4(1-\sqrt{2A/L})} - \frac{1}{4} \right) Z, \\ Z &= \log(\lambda_1^{a^2} \lambda_2^{b^2} \lambda_3^{c^2}). \end{aligned} \quad (8)$$

Here, $\tilde{\rho}^c$ is the mass density of collagen, N is the density of chains, and a, b and c are lengths of the unit cell sides aligned with the principal stretch directions. The material model is isotropic only if $a = b = c$.

The elastic stretches along the unit cell axes are respectively denoted by λ_1, λ_2 and λ_3 . $C^e = F^{eT} F^e$ is the elastic right Cauchy-Green strain tensor of collagen and $\mathbf{1}$ is the second-order isotropic tensor. The factors γ and β control bulk compressibility that models the extra-cellular fluid bound to proteoglycans. The end to end chain length is given by $r = \frac{1}{2} \sqrt{a^2 \lambda_1^2 + b^2 \lambda_2^2 + c^2 \lambda_3^2}$, where $\lambda_I = \sqrt{N_I \cdot C^e N_I}$, and $N_I, I = 1, 2, 3$ are the unit vectors along the three unit cell axes, respectively. The parameters introduced in (8) have been fit to data from Bischoff et al (2002) for our preliminary computations that appear below in Section 4.

3.2 A nearly incompressible ideal fluid

In our preliminary work, the fluid phase is treated as a nearly incompressible, ideal, i.e., inviscid, fluid. This is modelled by utilising an internal energy density function whose dependence on $\det(F^{ef})$ is quadratic, and the resulting partial Cauchy stress in the fluid is

$$\sigma^f = \det(F^{ef})^{-1} P^f F^{efT} = h(\rho^f) \mathbf{1}, \quad (9)$$

where a large value of h ensures near-incompressibility.

3.2.1 Response of the fluid in tension; cavitation

The response of the ideal fluid, as defined by Equation (9), does not explicitly distinguish between the cases where the

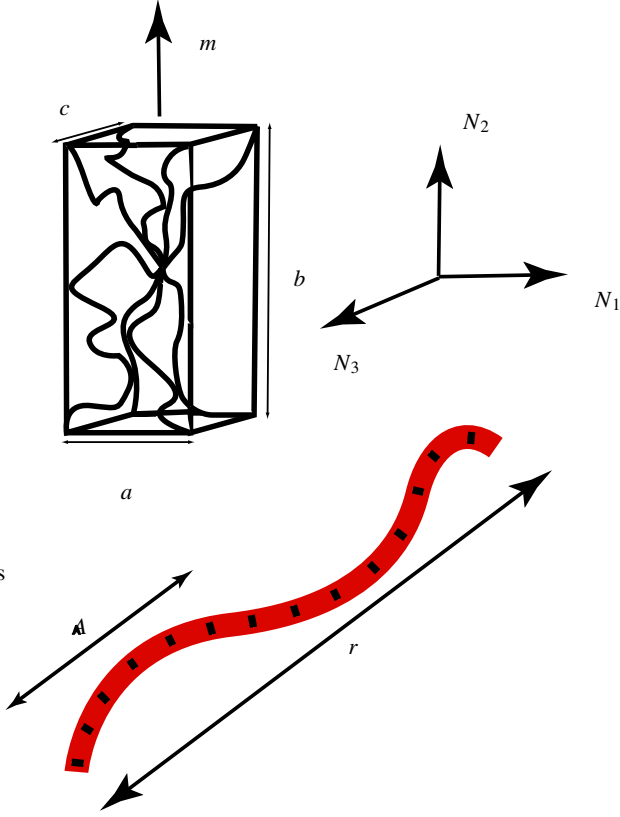


Fig. 5 The eight-chain model incorporating worm-like chains.

fluid is subjected to tension or compression, i.e., whether $\det(F^{e^f}) \geq 1$. When the fluid phase is subjected to compression, being (nearly) incompressible, it can develop compressive stresses without bound and is modelled accurately. Under tension, in actuality, the fluid can develop at most a small tensile stress, and the bulk of the tensile stiffness arises from the collagen phase. This is not accurately represented by using (9), which predicts a tensile response in fluid similar to the compressive response.

This is corrected by limiting $\det(F^{e^f}) \leq 1$, i.e., limiting the usage of the fluid stress response law only to the compressive case. In order to do this consistently, we first introduce an additional component to the mixture, a *void* species, v . Now, we only require that the product $\det(F^{e^f})\det(F^v)$ be equal to the determinant of the local deformation gradient. If this product tends to be ≥ 1 , we limit the $\det(F^{e^f})$ to 1, and the remainder is carried in $\det(F^v)$. Otherwise, $\det(F^v)$ is defined to be 1. In this manner, we allow the system to cavitate ($\det(F^v) > 1$), and this additionally gives us a measure of the unsaturation in the system.

3.3 Constitutive relations for fluxes

The constitutive relation for the flux of extra-cellular fluid relative to the collagen takes the following form,

$$M^f = D^f \left(\rho_0^f F^T g + F^T \text{DIV} [P^f] - \text{GRAD} [e^f - \theta \eta^f] \right), \quad (10)$$

where D^f is the positive semi-definite mobility of the fluid and isothermal conditions are assumed to approximate the physiological ones. Experimentally determined transport coefficients (e.g. for rat tail skin (Swartz et al, 1999) and rabbit Achilles tendons (Han et al, 2000)) are used for the fluid mobility values. The terms in the parenthesis on the right hand-side of Equation (10) sum up to give the total driving force for transport. The first term is the contribution due to gravitational acceleration. The second term arises from stress divergence; for instance, fluid moves down a compressive pressure gradient, which is Darcy's Law. The third term can be thought of as the gradient of a chemical potential. The included entropy gradient in this term results in classical Fickian diffusion if only mixing entropy exists. For a detailed derivation and discussion of Equation (10), the reader is directed to Garikipati et al (2004).

Additionally, during the course of implementing the theory and solving initial-boundary value problems, some refinements to the above constitutive relation have made themselves apparent. One such change is the splitting of permeability (stress-gradient driven) and diffusion (Fickian) mobilities, which proves useful, as seen in the following subsection.

3.3.1 Saturation and Fickian diffusion

Only when pores are unsaturated are there multiple configurations available to the fluid molecules at a fixed fluid concentration. This leads to a non-zero mixing entropy. In contrast, if saturated, there is only a single available configuration (degeneracy), resulting in zero mixing entropy. Consequently, Fickian diffusion, which arises from the gradient of mixing entropy can exist only in the unsaturated case. Even so, a saturated pore structure can demonstrate concentration gradient-dependent transport phenomenologically: The fluid stress depends on fluid concentration, see Equation (9), and fluid stress gradient-driven flux appears as concentration gradient-driven flux.

The saturation dependence of Fickian diffusion is modelled by using the measure of saturation introduced in Subsection 2.2.1, and switching on the diffusion (Fickian) mobility introduced above only if the tissue is unsaturated.

3.3.2 Transport of solute species

The numerous dissolved solute species (proteins, sugars, nutrients, ...), denoted by s , undergo large scale transport primarily by being advected along with the perfusing fluid. In addition to this, they are also capable of undergoing transport relative to the fluid. Toward this end, an additional velocity split of the form $V^s = \widetilde{V}^s + V^f$, is introduced, where \widetilde{V}^s now denotes the velocity of the solute relative to the fluid. The constitutive relation for the corresponding flux, denoted

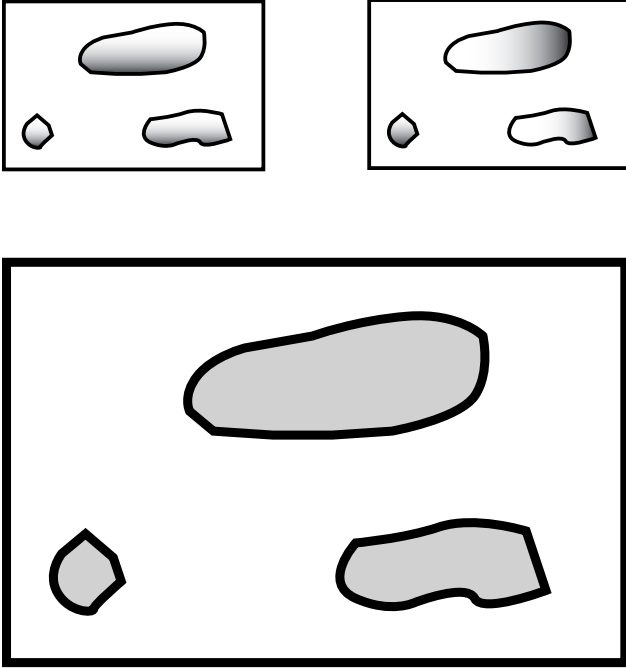


Fig. 6 Only unsaturated tissues can undergo Fickian diffusion.

by \tilde{M}^s , has the following form similar to Equation (10) defined for the fluid flux.

$$\tilde{M}^s = D^s (\rho_0^s F^T g - \text{GRAD}[e^s - \theta \eta^s]), \quad (11)$$

where D^s is the positive semi-definite mobility of the solute relative to the fluid, and again, isothermal conditions are assumed to approximate the physiological ones. Being in solution, this phase does not bear appreciable stress, and the stress divergence term is absent from the constitutive relation.

3.3.3 Objectivity and the contribution from acceleration

In our earlier treatment (Garikipati et al, 2004), the constitutive relation for the fluid flux had a driving force contribution arising from the acceleration of the solid phase, $-\rho_0^f F^T \frac{\partial V}{\partial t}$. This term, motivated by the reduced dissipation inequality, does not violate the Second Law and supports our intuitive understanding that accelerating the solid skeleton in one direction must result in an inertial driving force on the fluid in the opposite direction. However, as defined, this acceleration is obtained by the time differentiation of kinematic quantities³, and does not transform in an objective

³ and not in terms of acceleration *relative to fixed stars*, for e.g., as discussed in Truesdell and Noll (1965).

(frame-indifferent) manner under a change of frame. Unlike the superficially similar term arising from the gravity vector⁴, the acceleration term presents an improper dependence on the frame of the observer. Thus, its use in constitutive relations is inappropriate, and the term has been dropped in Equation (10).

3.3.4 Incompressible fluid in a porous solid

Upon incorporation of the velocity split described in Subsection 3.3.2, the resulting mass transport equation for the solute species is of an advection-diffusion form. In the hyperbolic limit, where advection dominates, spatial oscillations are observed in numerical solutions of this equation (Brooks and Hughes, 1982; Hughes et al, 1987). However, the form in which the equation is obtained is not amenable for the application of standard stabilisation techniques (Hughes et al, 1987). Additionally, though the (near) incompressibility of the fluid phase is imbibed in the balance of linear momentum, it has not yet been explicitly incorporated into the transport equations. This subsection proceeds to impose the fluid incompressibility condition and deduces implications for the solute mass transport equation, including a crucial simplification allowing for its straightforward numerical stabilisation.

From Equation (3), the local form of the balance of mass for the fluid species (recalling that $\Pi^f = 0$) in the current configuration is

$$\frac{d\rho^f}{dt} = -\text{div}[m^f] - \rho^f \text{div}[v]. \quad (12)$$

In order to impose the incompressibility of the fluid, we first denote by $\rho_{0\text{ini}}^f$ the *initial* value of the fluid reference density, and recognise that

$$\begin{aligned} \rho_0^f(X, 0) &=: \rho_{0\text{ini}}^f(X) \\ &= \rho_{\text{ini}}^f(x \cdot \varphi) J(X) \\ &= \frac{\rho^f(x \cdot \varphi, t)}{J^f_g(X, t)} J(X, t) \\ &= \rho^f(x \cdot \varphi, t) J^{\neq c}(X, t) \approx 1 \text{ for all time } t \end{aligned} \quad (13)$$

which results in a very high mobility in response to a pressure gradient, due to near incompressibility. Restricting the argument to a non-growing solid, i.e. F in the solid and $F^{\neq c}$ are uniform,

$$\frac{\partial}{\partial t} (\rho_{0\text{ini}}^f(X)) \equiv 0 \Rightarrow \frac{\partial}{\partial t} (\rho^f(x \cdot \varphi, t)) = 0, \quad (14)$$

which is the hidden implication of our assumption that F is the deformation gradient of the system and of the solid

⁴ where every observer has an implicit knowledge of the directionality of the field relative to a fixed frame, allowing it to transform objectively.

skeleton. This leads to $\frac{\partial \rho^f}{\partial t} = 0$, as seen in our numerical simulations. We now proceed to treat our fluid mass transport at steady state. Rewriting the flux m^f from Equation (12) as the product $\rho^f v^f$ and using the result derived above,

$$\begin{aligned} 0 &= \frac{\partial \rho^f}{\partial t} \Big|_X \\ &= -\text{div} [\rho^f v^f] - \rho^f \text{div} [v]. \end{aligned} \quad (15)$$

Returning to (3), we introduce the additional velocity split, $V^s = \widetilde{V}^s + V^f$, and now write the balance mass for a solute species as

$$\begin{aligned} \frac{d\rho^s}{dt} &= \pi^s - \text{div} \left[\widetilde{m}^s + \frac{\rho^s}{\rho^f} m^f \right] - \rho^s \text{div} [v] \\ &= \frac{\rho^s}{\rho^f} \left(-\text{div} [\rho^f v^f] - \rho^f \text{div} [v] \right) \\ &\quad + \pi^s - \text{div} [\widetilde{m}^s] - m^f \cdot \text{grad} \left[\frac{\rho^s}{\rho^f} \right]. \end{aligned} \quad (16)$$

Thus, using the incompressibility condition (15), we get the simplified form of the balance of mass for an arbitrary solute species, s ,

$$\frac{d\rho^s}{dt} = \pi^s - \text{div} [\widetilde{m}^s] - \frac{m^f \cdot \text{grad} [\rho^s]}{\rho^f} + \frac{\rho^s m^f \cdot \text{grad} [\rho^f]}{\rho^{f^2}}. \quad (17)$$

This is now in standard advective-diffusion form, and is well suited for stabilisation schemes such as the streamline upwind Petrov-Galerkin (SUPG) method (see, for e.g., Hughes et al (1987)) described briefly below.

3.3.5 Stabilisation of the simplified solute transport equation

SUPG methods are a class of finite element methods, originally developed for the scalar advection-diffusion equation, which have proven efficient in the solution of a variety of flow problems (Hughes, 1987). The standard form of the scalar advection-diffusion is

$$\frac{\partial \varphi}{\partial t} + a \cdot \text{grad} [\varphi] = \text{div} [\kappa \text{grad} [\varphi]] + f, \quad (18)$$

where $\varphi = \varphi(x, t)$ is a scalar field, a is the advective velocity, κ is a diffusivity and f is a volumetric source term. Here, if $\kappa > 0$, we have the parabolic case and if $\kappa = 0$, we have the hyperbolic case. In terms of numerics, the greatest challenge is posed when the element *Peclet number*,

$$\alpha = \max \frac{|a|h}{2\kappa}, \quad (19)$$

is large; h being the mesh size. Figure 7 shows the spatial instability in the numerical solution of a simple 2 dimensional case of (18), where the element Peclet number is large.

Recalling that the *material time derivative* on the left-hand side of Equation (17) is defined as follows,

$$\frac{d\rho^s}{dt} := \frac{\partial \rho^s}{\partial t} + \text{grad} [\rho^s] \cdot v, \quad (20)$$

where v is the material velocity of the solid skeleton, we compare the forms of (17) and (18) to determine the nature of the abstract quantities a and f for our problem.

In contrast to the standard Galerkin method, the SUPG offers a greater control over the advective-derivative term by adding an artificial diffusion which acts only along the direction of the streamline. The key idea here is that this stabilising control is introduced within a weighted residual format and maintains consistency (Hughes, 1987). In weak form, the method is defined as follows

$$\begin{aligned} &\int_{\Omega} \left(w^h a \cdot \text{grad} [\varphi^h] + \text{grad} [w^h] \cdot \kappa \text{grad} [\varphi^h] \right) d\Omega \\ &+ \sum_{e=1}^{n_{el}} \int_{\Omega_e} \tau a \cdot \text{grad} [w^h] \left(a \cdot \text{grad} [\varphi^h] - \text{div} [\kappa \text{grad} [\varphi^h]] \right) d\Omega \\ &= \int_{\Omega} w^h f d\Omega + \int_{\Gamma_h} w^h h d\Gamma + \sum_{e=1}^{n_{el}} \int_{\Omega_e} \tau a \cdot \text{grad} [w^h] f d\Omega \end{aligned} \quad (21)$$

where Γ_h is the Neumann boundary, and this equation introduces a numerical stabilisation parameter τ , which we have calculated from the L_2 norms of element level matrices, as described in Tezduyar and Sathe (2003). In Figure 8, the stable numerical solution of the sample high Peclet number problem introduced previously is shown after the introduction of this artificial diffusion.

3.4 Nature of the sources

There exists a large body of literature, Cowin and Hegedus (1976); Epstein and Maugin (2000); Ambrosi and Mollica (2002), that addresses growth in biological tissue mainly based upon a single species undergoing transport and production/annihilation. In actuality, growth depends on cascades of complex biochemical reactions involving several species, and additionally involves intimate coupling between mass transfer, biochemistry and mechanics. An example of this chemo-mechanical coupling is described in Provenzano et al (2003).

The modelling approach followed in this work is to select appropriate functional forms of the source terms for collagen, Π^c , and the solutes, Π^s , to suitably encapsulate the complexity of the biochemistry we aim to capture. In our earlier exposition (Garikipati et al, 2004), we utilised simple first order chemical kinetics to define Π^c . This has now been expanded to model more physiologically relevant forms of biochemistry, and the following subsections discuss two examples. We are currently looking at combinations of these sources, and aim to calibrate our choices from tendon growth experiments.

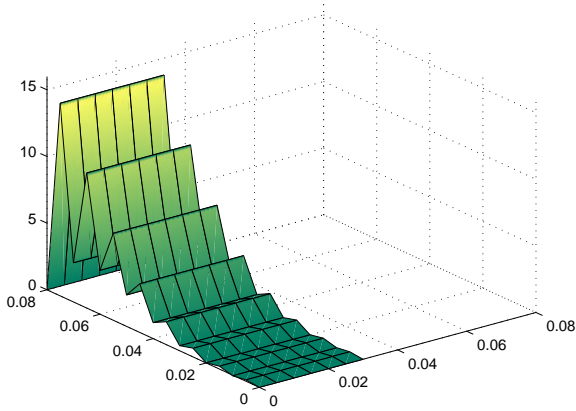


Fig. 7 Advection-diffusion equation solution with stabilisation term turned off

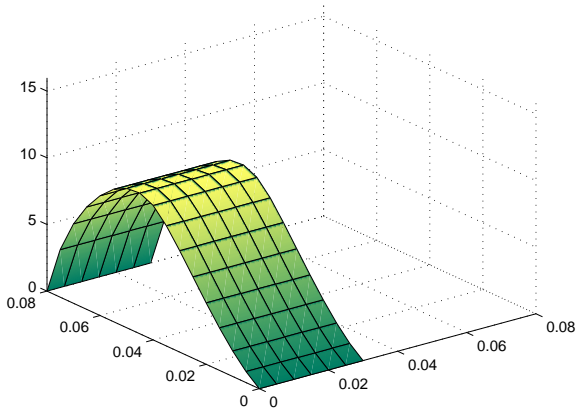


Fig. 8 Advection-diffusion equation solution with stabilisation term turned on

3.4.1 Enzyme kinetics

Michaelis-Menten enzyme kinetics (see, for e.g., Sengers et al (2004)) involves a two-step reaction with the collagen and solute production terms given by

$$\Pi^s = \frac{(k_{\max}\rho^s)}{(\rho_m^s + \rho^s)}\rho_{\text{cell}}, \quad \Pi^c = -\Pi^s, \quad (22)$$

where ρ_{cell} is the concentration of fibroblasts, k_{\max} is the maximum value of the solute production reaction rate constant, and ρ_m^s is half the solute concentration corresponding to k_{\max} . Denoting the two-stage reaction, involving an enzyme, substrate and a product, by $E + S \xrightleftharpoons[k_{-1}]{k_1} ES \xrightarrow{k_2} E + P$,

it can be shown that $\rho_m^s = \frac{(k_2 + k_{-1})}{k_1}$. Figure 9 shows a representative plot of initial reaction rate vs. the solute concentration.

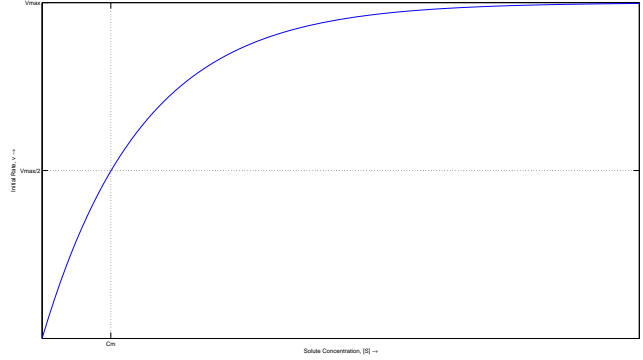


Fig. 9 Initial reaction rate vs. solute concentration in enzyme kinetics.

3.4.2 Strain energy dependent collagen production

The strain energy dependent source term was originally proposed in the context of bone growth (Harrigan and Hamilton, 1993) and induces growth at a point when the energy density deviates from a basal value, suitably weighted by a relative density ratio. Written for collagen, it has the form

$$\Pi^c = \left(\frac{\rho_0^c}{\rho_{0_{\text{ini}}^c}}\right)^{-m} \psi_F - \psi_F^*, \quad (23)$$

where ψ_F^* is a reference strain energy density.

4 Numerical examples

The theory presented in the preceding sections results in non-linear coupled partial differential equations that need to be solved. A finite element formulation employing a staggered scheme based upon operator splits Armero (1999); Garikipati and Rao (2001) has been implemented in FEAP Taylor (1999) to solve the coupled problem. The basic solution scheme involves keeping one of the fields, say the displacement field, fixed, while solving for another, the concentration field from the mass transport problem in this case. The resulting concentration field is then fixed to solve the mechanics problem. This procedure is repeated until the resulting fields satisfy the differential equations within some suitable magnitude of an error norm.

The transient solution for the mechanics problem is obtained using energy-conserving schemes as detailed in Simo and Tarnow (1992). Backward Euler is used as the time-stepping algorithm for mass transport. Non-linear projection methods (Simo et al, 1985) are used to treat the near-incompressibility imposed by water. Mixed methods, as described in Garikipati and Rao (2001), are used for stress (and strain) gradient driven fluxes.

The following example aims to demonstrate the mathematical formulation and aspects of the coupled phenomena as the tissue grows. The model geometry, based on the engineered tendon constructs (see Figure 10), is a cylinder 12 mm in length and 1 mm² in cross-sectional area. Only two phases—fluid and collagen—are included for the mass

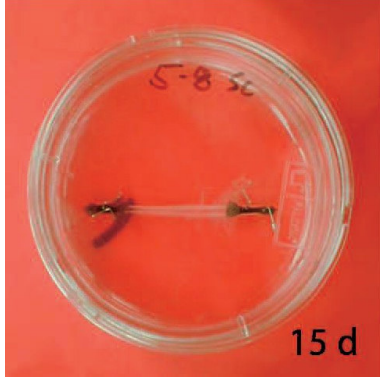


Fig. 10 Engineered tendon constructs Calve et al (2004).

transport and mechanics. The collagen is represented by the anisotropic worm-like chain model outlined previously (see Section 3.1) and the fluid phase is modelled as ideal and nearly incompressible. The parameters used in the analysis are as presented in Table 2.1. The values chosen are representative of the kinds of biological systems we are working with. The classes of initial and boundary conditions imposed are also based on physical experiments.

Since we only have two species and we want to demonstrate growth, an “artificial” fluid sink Π^f is introduced following simple first order kinetics. The collagen source will be the negative of the fluid sink: $\Pi^f = -k^f(\rho_0^f - \rho_{0_{ini}}^f)$; $\Pi^c = -\Pi^f$, where k^f is the reaction rate, and $\rho_{0_{ini}}^f$ is the initial concentration of fluid. When $\rho_0^f > \rho_{0_{ini}}^f$, this acts as a source for collagen. The mixing entropy of fluid in the mixture with collagen is written as $\eta_{mix}^f = -\frac{k}{\mathcal{M}^f} \log(\frac{\rho_0^f}{\rho_0})$, where \mathcal{M}^f is the molecular weight of the fluid.

The boundary conditions simply corresponding to immersing the tendon in a nutrient rich bath. The initial collagen concentration is 500 kg/m^3 everywhere and the fluid concentration is 400 kg/m^3 everywhere. This is exposed to a bath where the fluid concentration is 500 kg/m^3 , so with these concentration boundary conditions set, nutrient rich fluid rushes into the tissue, and growth occurs to form more collagen. The following plots present a few results from the analysis.

4.1 Effects of non-physical boundary conditions

4.2 The constriction induced growth problem

4.3 A swelling problem

Figure 11 shows the initial collagen concentration in the tendon. After it has been immersed in a nutrient rich bath for half an hour, the tendon has grown and the collagen concentration is now higher as seen in Figure 12. On performing a simple uniaxial tension test on the tendon before and after growth, it is observed that the grown tissue is stiffer and stronger as seen in Figure 13. Additionally, the swelling

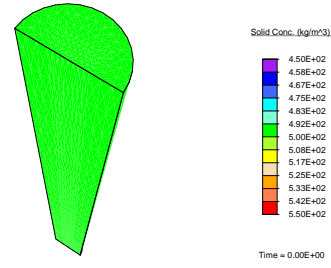


Fig. 11 The collagen concentration (kg/m^3) initially.

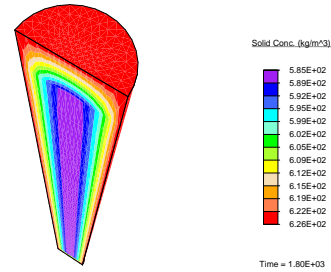


Fig. 12 The collagen concentration (kg/m^3) after 1800 seconds.

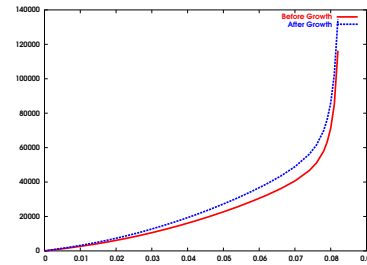


Fig. 13 The stress (Pa) vs extension (m) curves before and after growth.

of the tendon as it is immersed in the bath takes place in two clear regimes as seen in Figure 14. There is an initial rapid swelling in a diffusion dominated regime, and a slower growth dominated swelling later on.

4.4 An enzyme-kinetics based multiphasic problem

5 Conclusion

In this paper, we have discussed in detail a number of enhancements to our original growth formulation presented in Garikipati et al (2004). That formulation has demonstrated its versatility and power as a platform for posing a very wide range of questions on the biophysics of growth. Some issues, such as saturation, incompressibility of the fluid species and its influence upon the tissue response, and the roles of biochemical and strain energy-dependent source terms are specific to soft biological tissues. We note, however, that other issues are also applicable to a number of systems with a porous solid, transported fluid and reacting solutes. Included

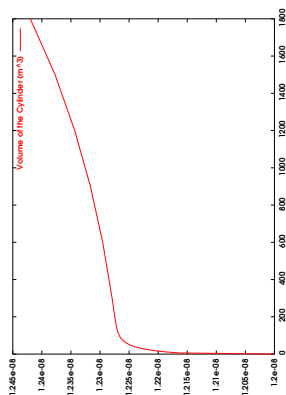


Fig. 14 The volume of the tendon (m^3) evolving with time.

in these are issues of current versus reference configurations for mass transport, swelling, Fickian diffusion, fluid response in compression and tension, cavitation, and role of different mobilities.

These issues have been resolved using simple, but powerful arguments that could be posed easily in the framework derived in Garikipati et al (2004). However, the interactions engendered in the coupled reaction-transport-mechanics system are complex, as borne out by the numerical examples in Section 4. The treatment of these issues has led to a formulation more suited to the biophysics of growing soft tissue, making progress toward our broader goal of applying it to applications such as the study of wound healing, pathological hypertrophy/atrophy, as well as drug efficacy and interaction.

References

- Ambrosi D, Mollica F (2002) On the mechanics of a growing tumor. *Int J Engr Sci* 40:1297–1316
- Armero F (1999) Formulation and finite element implementation of a multiplicative model of coupled poroplasticity at finite strains under fully-saturated conditions. *Comp Methods in Applied Mech Engrg* 171:205–241
- Arruda EM, Boyce MC (1993) A three-dimensional constitutive model for the large stretch behavior of rubber elastic materials. *Journal of Mechanics and Physics of Solids* 41:389–412
- Bischoff JE, Arruda EM, Grosh K (2002) A microstructurally based orthotropic hyperelastic constitutive law. *J Applied Mechanics* 69:570–579
- Brooks A, Hughes T (1982) Streamline upwind/Petrov-Galerkin formulations for convection dominated flows with particular emphasis on the incompressible Navier-Stokes equations. *Comp Methods in Applied Mech Engrg* 32:199–259
- Bustamante C, Bryant Z, Smith SB (2003) Ten years of tension: Single-molecule DNA mechanics. *Nature* 421:423–427
- Calve S, Dennis R, Kosnik P, Baar K, Grosh K, Arruda E (2004) Engineering of functional tendon. *Tissue Engineering* 10:755–761
- Cowin SC, Hegedus DH (1976) Bone remodeling I: A theory of adaptive elasticity. *Journal of Elasticity* 6:313–325
- Epstein M, Maugin GA (2000) Thermomechanics of volumetric growth in uniform bodies. *International Journal of Plasticity* 16:951–978
- Fung YC (1993) *Biomechanics: Mechanical properties of living tissues*, 2nd edn. Springer-Verlag, New York
- Garikipati K, Rao VS (2001) Recent advances in models for thermal oxidation of silicon. *Journal of Computational Physics* 174:138–170
- Garikipati K, Arruda EM, Grosh K, Narayanan H, Calve S (2004) A continuum treatment of growth in biological tissue: Mass transport coupled with mechanics. *Journal of Mechanics and Physics of Solids* 52:1595–1625
- Graham JS, Vomund AN, Phillips CL, Grandbois M (2004) Structural changes in human type I collagen fibrils investigated by force spectroscopy. *Experimental Cell Research* 299:335–342
- Han S, Gemmell SJ, Helmer KG, Grigg P, Wellen JW, Hoffman AH, Sotak CH (2000) Changes in ADC caused by tensile loading of rabbit achilles tendon: Evidence for water transport. *Journal of Magnetic Resonance* 144:217–227
- Harrigan TP, Hamilton JJ (1993) Finite element simulation of adaptive bone remodelling: A stability criterion and a time stepping method. *Int J Numer Methods Engrg* 36:837–854
- Hughes T, Franca L, Mallet M (1987) A new finite element formulation for computational fluid dynamics: VII. Convergence analysis of the generalized SUPG formulation for linear time-dependent multidimensional advective-diffusive systems. *Comp Methods in Applied Mech Engrg* 63(1):97–112
- Hughes TJR (1987) Recent progress in the development and understanding of SUPG methods with special reference to the compressible Euler and Navier-Stokes equations. *International Journal for Numerical Methods in Fluids* 7:1261–1275
- Kratky O, Porod G (1949) Röntgenuntersuchungen gelöster Fadenmoleküle. *Recueil Trav Chim* 68:1106–1122
- Kuhl E, Steinmann P (2003) Theory and numerics of geometrically-nonlinear open system mechanics. *Int J Numer Methods Engrg* 58:1593–1615
- Landau LD, Lifshitz EM (1951) *A Course on Theoretical Physics, Volume 5, Statistical Physics, Part I*. Butterworth Heinemann (reprint)
- Lee EH (1969) Elastic-Plastic Deformation at Finite Strains. *J Applied Mechanics* 36:1–6
- Marko JF, Siggia ED (1995) Stretching DNA. *Macromolecules* 28:8759–8770
- Provenzano PP, Martinez DA, Grindeland RE, Dwyver KW, Turner J, Vailas AC, Vanderby R (2003) Hindlimb unloading alters ligament healing. *Journal of Applied Physiology* 94:314–324

- Rief M, Oesterhelt F, Heymann B, Gaub HE (1997) Single Molecule Force Spectroscopy of Polysaccharides by Atomic Force Microscopy. *Science* 275:1295–1297
- Sengers BG, Oomens CWJ, Baaijens FPT (2004) An integrated finite-element approach to mechanics, transport and biosynthesis in tissue engineering. *J Bio Mech Engrg* 126:82–91
- Simo JC, Tarnow N (1992) Exact energy-momentum conserving algorithms and symplectic schemes for nonlinear dynamics. *Comp Methods in Applied Mech Engrg* 100:63–116
- Simo JC, Taylor RL, Pister KS (1985) Variational and projection methods for the volume constraint in finite deformation elasto-plasticity. *Comp Methods in Applied Mech Engrg* 51:177–208
- Sun YL, Luo ZP, Fertala A, An KN (2002) Direct quantification of the flexibility of type I collagen monomer. *Biochemical and Biophysical Research Communications* 295:382–386
- Swartz M, Kaipainen A, Netti PE, Brekken C, Boucher Y, Grodzinsky AJ, Jain RK (1999) Mechanics of interstitial-lymphatic fluid transport: Theoretical foundation and experimental validation. *J Bio Mech* 32:1297–1307
- Taber LA, Humphrey JD (2001) Stress-modulated growth, residual stress and vascular heterogeneity. *J Bio Mech Engrg* 123:528–535
- Taylor RL (1999) FEAP - A Finite Element Analysis Program. University of California at Berkeley, Berkeley, CA
- Tezduyar T, Sathe S (2003) Stabilization parameters in SUPG and PSPG formulations. *Journal of Computational and Applied Mechanics* 4:71–88
- Truesdell C, Noll W (1965) *The Non-linear Field Theories* (Handbuch der Physik, band III). Springer, Berlin